

2019-09-30

Antibacterial properties of silver nanoparticles grown in situ and anchored to titanium dioxide nanotubes on titanium implant against *Staphylococcus aureus*

Gunpath, UF

<http://hdl.handle.net/10026.1/14990>

10.1080/17435390.2019.1665727

Nanotoxicology

Taylor & Francis

All content in PEARL is protected by copyright law. Author manuscripts are made available in accordance with publisher policies. Please cite only the published version using the details provided on the item record or document. In the absence of an open licence (e.g. Creative Commons), permissions for further reuse of content should be sought from the publisher or author.

1 **Antibacterial properties of silver nanoparticles grown *in situ* and**
2 **anchored to titanium dioxide nanotubes on titanium implant against**
3 ***Staphylococcus aureus***

4 Urvashi F. Gunpath ^{1,2}, Huirong Le ^{2*}, Kiruthika Natesan³, Alexandros Besinis ¹,
5 Christopher Tredwin ³ and Richard D. Handy ^{4*}

6 ¹*School of Engineering, Plymouth University, Plymouth, PL4 8AA, United Kingdom*

7 ²*School of Mechanical Engineering and Built Environment, University of Derby, DE22*
8 *3AW, United Kingdom*

9 ³*Peninsula Schools of Medicine and Dentistry, Plymouth University, Research Way,*
10 *Plymouth, Devon, PL6 8BU, United Kingdom*

11 ⁴*School of Biological & Marine Sciences, Plymouth University, PL4 8AA, United*
12 *Kingdom*

13 Corresponding Authors: r.handy@plymouth.ac.uk (R. D. Handy) and h.le@derby.ac.uk (H. R.
14 Le).

15

16 **Abstract**

17 Medical grade titanium alloy, Ti-6Al-4V, with TiO₂ nanotubes (TiO₂-NTs) grown
18 on the surface and then decorated with silver nanoparticles (Ag NPs) is proposed to
19 enhance the antimicrobial properties of the bone/dental implants. However, the
20 decoration with Ag NPs is not consistent and there are concerns about the direct
21 contact of Ag NPs with human tissue. The aim of this study was to achieve a more
22 even coverage of Ag NPs on TiO₂-NTs and determine their biocidal properties
23 against *Staphylococcus aureus*, with and without a top coat of nano hydroxyapatite
24 (nHA). The decoration with Ag NPs was optimised by adjusting the incubation time
25 of the TiO₂-NTs in a silver ammonia solution, and using biocompatible δ -
26 gluconolactone as a reducing agent. The optimum incubation in silver ammonia
27 was 7 minutes, and resulted in evenly distributed Ag NPs with an average diameter
28 of 47.5 ± 1.7 nm attached to the surface of the nanotubes. The addition of nHA did
29 not compromise the antimicrobial properties of the materials; high resolution
30 electron microscopy showed *S. aureus* did not grow on the composite with nHA
31 and with >80 % biocidal activity measured by the LIVE/DEAD assay, also limited
32 lactate production. Dialysis experiment confirmed the stability of the coatings, and
33 showed a slow release of dissolved silver (3.27 ± 0.15 $\mu\text{g/L}$ over 24 h) through the
34 top coat of nHA.

35

36 Keywords: Silver nanoparticles, titanium dioxide nanotubes, nano hydroxyapatite,
37 *Staphylococcus aureus*, antimicrobial, silver dissolution

38

39

40

41

42

43

44

45

46 **Introduction**

47 Orthopaedic and dental implants should be suitably durable with mechanical properties
48 that mimic the intended tissue (O'Brien, 2011). The implants must also be biocompatible
49 and ideally exhibit some antimicrobial properties as infection post-surgery is an
50 underlying cause of implant failure (Connaughton *et al.*, 2014). The challenge is to make
51 a medical implant with all these attributes. Titanium dioxide nanotubes (TiO₂-NTs) are
52 readily grown on medical grade titanium whereby they can resist mechanical stresses
53 similar to those faced by bone (Descamps *et al.*, 2013). They have also been shown to be
54 biocompatible with bone cells, partly because they mimic the surface morphology of bone
55 (Brammer *et al.*, 2012). Crucially the properties of TiO₂-NTs can be tuned to the clinical
56 application by varying the thickness, surface texture and/or decoration of the nanotubes
57 (Spriano *et al.*, 2018). The relationship between the surface properties of TiO₂-NTs and
58 mechanistic responses of osteoblast cells is also partially understood (Meyerink *et al.*,
59 2018). However, TiO₂-NTs alone are not antimicrobial (Zhao *et al.*, 2011).

60 *Staphylococcus aureus* is one of the most common cause of infection in implants
61 (Rodríguez-Cano *et al.*, 2014). To enhance antimicrobial properties, TiO₂-NTs can be
62 coated with antibiotics such as gentamicin (Yang *et al.*, 2016) or vancomycin (Zhang *et*
63 *al.*, 2013). However, infections related to implants are normally caused by a mixture of
64 microbes (Nie *et al.*, 2017) and individual antibiotics are inevitably only targeted at a few
65 of the organisms present. There is also the concern of antibiotic resistance (Moriarty *et*
66 *al.*, 2016). Alternatively, dissolved metals such as silver, copper and zinc have been
67 known for their antimicrobial properties for centuries. Their solubility and biological
68 reactivity have restricted their applications to simple disinfectants in the past, but now
69 nanoparticulate forms of these metals are available. Of these metals, silver nanoparticles
70 (Ag NPs, review, Reidy *et al.*, 2013) are arguably the strongest biocide with minimum

71 inhibitory concentrations (MIC) for growth of 3.25 mg/l to *S. mutans* (Besinis *et al.*,
72 2014a). Ag NPs are also toxic to *S. sanguinus* when presented as a silver coating on
73 medical grade titanium alloy (Besinis *et al.*, 2017). However, the rapid release of Ag from
74 silver-containing coatings may cause toxicity to mammalian cells (Gao *et al.*, 2014), and
75 instead a controlled release of Ag by enhancing the stability of the coating is desirable
76 (Zhao *et al.*, 2011).

77 It is also possible to decorate Ag NPs onto the surface of TiO₂-NTs using
78 anodization methods (Gunpath *et al.*, 2018), and then add another biocompatible material
79 to control the Ag release. TiO₂-NTs can also be decorated with Ag NPs in the presence
80 of calcium phosphate NPs (Chernozem *et al.*, 2019), but there are some concerns about
81 the elastic properties and nanohardness of the implant material when Ca₃(PO₄)₂ is used
82 (Chernozem *et al.*, 2017). One possible alternative approach is to ‘top-coat’ the silver-
83 containing nanomaterial with a layer of biocompatible hydroxyapatite (HA), so that there
84 is no hazard to the human tissue and better mechanical properties. Hydroxyapatite (HA)
85 has a similar structure to bone and is well-known as a biocompatible material that
86 promotes osteointegration (Ramires *et al.*, 2001, Balani *et al.*, 2007). Nano forms of HA
87 (nHA) are also available (Ha *et al.*, 2015). Our previous work developed an anti-bacterial
88 coating consisting of TiO₂-NTs grown on Ti-6Al-4V alloy, with clusters of Ag NPs on
89 the TiO₂-NT surface (Gunpath *et al.*, 2018). The aim of the present study was to develop
90 these coatings further by optimising the incubation time with reducing agents to provide
91 a more uniform decoration of Ag NPs, and crucially, to determine if antibacterial
92 properties remained after top coating the materials with nHA. To demonstrate the
93 antimicrobial properties, the final composite coatings were tested against *S. aureus*. For
94 these latter studies, this included counting the proportions of live and dead bacteria on the

95 coatings, monitoring microbial activity with a lactate production assay, as well as electron
96 microscopy to observe coating integrity and the presence of any microbes.

97 **Materials and Method**

98 Titanium dioxide nanotubes (TiO₂-NTs) were self-assembled on the surface of Ti-6Al-
99 4V alloy discs followed by the chemical reduction of silver to form Ag NPs on the
100 nanotubes. For some of the silver coated nanotubes, nHA was sintered to the composite
101 coating. After characterising the different coatings formed, the antibacterial properties of
102 all of them were tested in the presence of *S. aureus*.

103 ***Growth of TiO₂-NTs with Ag NPs and HA coating***

104 The synthesis of the composite coatings started with TiO₂-NTs followed by the addition
105 of Ag NPs and last nHA. To start with, the self-assembly of the TiO₂-NTs on to titanium
106 alloy discs was conducted using an anodisation process as previously optimised
107 (Danookdharree *et al.*, 2015). Briefly, this was a 1 hour electrochemical reaction in a
108 mixture of 1 mol/L NH₄HPO₄ and 0.5 wt% NH₄F (0.5 g of NH₄F in 100 mL of ammonia
109 solution) at 20 V. All the coated discs were then annealed at 350 °C for 2 h in a furnace
110 to achieve the anatase phase (Carbolite RWF 1200, Carbolite Engineering Services, Hope
111 Valley, UK). The TiO₂-NTs were then functionalised by treating them with 2 mol/L
112 NaOH at 50 °C for 2 minutes (Parcharoen *et al.*, 2014). This resulted in the formation of
113 sodium titanate (Na₂Ti₃O₇) which is a reactive surface for the next steps in the synthesis
114 of the composite material.

115 Silver nanoparticles were then chemically reduced on the surface of the TiO₂-NTs
116 as previously described (Gunpath *et al.*, 2018). Briefly, a silver ammonia solution was
117 prepared, at room temperature and with continuous stirring, by mixing 2.545 g of silver
118 nitrate and 900 mL of ultrapure water, followed by 15 mL of 1 M NaOH. A precipitate

119 of silver oxide formed, but was continuously mixed to remain in suspension.
120 Concentrated liquid ammonia (13.4 M; density, 0.910 kg/m³) was then added dropwise
121 to the mixture until all the oxide had dissolved. Pure water was then added to bring the
122 final volume to 1000 mL. The resulting solution of silver ammonia, [Ag(NH₃)₂]⁺, (15
123 mM) was allowed to stir for a further 10 minutes to ensure complete reaction and mixing.
124 Afterwards, 2 mM δ-gluconolactone solution (Sigma Aldrich, UK) was prepared in 12
125 mM NaOH, the volume of which was dependent on the experiment performed.

126 The titanium alloy discs covered with TiO₂-NTs were immersed in silver ammonia
127 first, allowing the cationic silver ammonia to attach to –O⁻ residues of the nanotubes
128 (Gunpath *et al.*, 2018). After an initial exposure to the silver ammonia, the samples were
129 ultrasonicated in deionised water at 12 MHz for 5 minutes to remove any loosely attached
130 silver ammonia; after which the disks were air dried at room temperature. The samples
131 were then exposed to the gluconolactone solution for 5 minutes. Depending on the
132 exposure time to silver ammonia, the samples were identified as TiO₂-Ag3, TiO₂-Ag7
133 and TiO₂-Ag10 for an exposure of 3, 7 and 10 minutes in silver ammonia respectively,
134 and all treated for 5 minutes in gluconolactone solution (n = 3 each). Gluconolactone was
135 expected to reduce the silver ammonia to Ag NPs which are attached on the surface of
136 the TiO₂-NTs. The samples were again ultrasonicated in deionised water for 5 minutes
137 with the aim of removing the loosely attached Ag NPs.

138 After the optimisation of the incubation time for the synthesis of Ag NPs on the
139 TiO₂-NT discs, hydroxyapatite was finally added using a sintering method (Besinis *et al.*,
140 2017). Briefly, 7 minutes was deemed the optimum time for the silver ammonia
141 treatment, and so TiO₂-Ag7 discs were placed in 24-well plates and sterilised with 70 %
142 ethanol (n = 12 discs). Afterwards, 20 µL of 10 wt% nHA solution (Sigma Aldrich, UK)
143 was evenly pipetted on top of the discs after which they were left to dry at room

144 temperature for 48 hours. Subsequently, the discs were placed in a porcelain dish and
145 gradually heated (Carbolite furnace, Hope, UK) at 10 °C per min to 500 °C. The final
146 temperature was maintained for 10 minutes after which the temperature was gradually
147 reduced to room temperature. The 500 °C temperature was chosen as it was high enough
148 to cause sintering, while being below the melting point of silver. The change in
149 temperature was gradual to ensure maintaining the crystallinity of the nHA. The resulting
150 discs are hereafter termed 'TiO₂-Ag7-HA'.

151

152 ***Characterisation of the coatings***

153 The morphology and chemical composition of the TiO₂ at each step of the synthesis (i.e.,
154 addition of Ag-NPs and then HA) was analysed by scanning electron microscopy with
155 energy dispersive spectroscopy (SEM/EDS). Figure 1 shows the surface morphology
156 prior to the HA additions and for different incubations times with silver ammonia. The
157 growth of the TiO₂-NTs gave generally good coverage of the alloy, as expected
158 (Danookdharree *et al.*, 2015). When 3 minutes incubation time was used (TiO₂-Ag3), the
159 TiO₂-NTs had less spherical Ag NPs on the surface (Figure 1B). The samples incubated
160 for 7 minutes (TiO₂-Ag7) had a more uniform distribution of Ag NPs. In both TiO₂-Ag3
161 and TiO₂-Ag7, the nanotubular characteristic of the TiO₂ was still visible after the growth
162 of Ag NPs. However in TiO₂-Ag10, the Ag NPs grown covered the whole surface of the
163 TiO₂ with some clustering observed (Figure 1D). The EDS analysis of the white spherical
164 nanoparticles on the discs confirmed the presence of silver with the weight percentage of
165 the latter over the coating increasing from TiO₂-Ag3 to TiO₂-Ag10 (5-8 wt%) to the
166 contrary of Ti, Al and O which were found to be decreasing. The incubation time also
167 affected the primary size of the Ag NPs, as observed by electron microscopy, with
168 diameters of 88.25 ± 5.1 , 47.5 ± 1.7 , 30 ± 2.4 nm for incubations of 3, 7 and 10 minutes

169 with silver ammonia, respectively (all significantly different from each other, ANOVA,
170 $P < 0.05$).

171 For the logistics of biological testing, one 'best' composite had to be selected for
172 experimental work. After considering all the characterisation information, TiO₂-Ag7 was
173 chosen as the coated samples to be taken forward for further testing. This was selected on
174 the basis that it had the most uniform coating with almost no clustering of and full surface
175 coverage of the Ag NPs (Figure 2). After the addition of nHA to the latter coating, another
176 uniformly distributed coating was obtained (Figure 2B). The EDS analysis (Figure 2D)
177 confirms the presence of Ca and P as part of the nHA. As expected, the amount of silver
178 now detected with the HA surface was less than TiO₂-Ag7 alone (< 5 wt %). Some
179 cracking of the nHA layer was observed (Figure 2D), but this regarded as a desirable
180 feature to facilitate the slow release of the underlying silver.

181

182 ***Dialysis experiment and the release of dissolved metal***

183 A dialysis experiment was conducted according to Besinis *et al* (2014b) using the TiO₂-
184 Ag7 and TiO₂-Ag7-HA discs to inform on the release of any dissolved Ag with respect
185 to antibacterial properties, and on the stability of the coatings (Besinis *et al.*, 2014a). A
186 simulated body fluid (SBF) was used for these experiments (in mmol/l): Na⁺, 142; K⁺,
187 5.0; Mg²⁺, 1.5; Ca²⁺, 2.5; Cl⁻, 147.8; HCO₃⁻, 4.2; HPO₄²⁻, 1.0; SO₄²⁻, 0.5 (Kokubo *et al.*,
188 1990), with the pH adjusted to 7.2 with a few drops of 1 mol/L HCl. Experiments were
189 conducted in triplicate at room temperature in previously acid washed (5% nitric acid)
190 and deionised glassware. Dialysis tubing (MW cut off, 12 000 Da, Sigma Aldrich, UK),
191 was cut in 7 cm x 2.5 cm lengths and sealed at one end using a Mediclip; then filled with
192 one Ti alloy discs as appropriate with 7 mL of SBF. The dialysis bag was closed with
193 another Mediclip and then suspended in a 500 mL pyrex glass beaker containing 243 mL

194 of SBF (i.e., total volume 250 mL). The beakers were gently stirred throughout, and 4
195 mL aliquots of the SBF were collected from the external compartment of the beaker at 0,
196 0.5, 1, 2, 3, 4, 6, 8, 24 h. The SBF samples were acidified with a drop of 70 wt% nitric
197 acid and stored for metal analysis (see below). At the end of the 24 h, the dialysis bags
198 were also carefully opened and 4 ml of the fluid therein collected for metal analysis.
199 Dialysis curves were plotted using SigmaPlot 13.0 (Systat Software, Inc.), after deducting
200 the background ionic concentrations of the SBF. A first order rectangular hyperbola
201 function was used to fit dialysis curves to the raw data. The maximum initial slope of the
202 curves informed on the maximum apparent dissolution rate of each substance.

203

204 ***Plate preparation and exposure to *S. aureus****

205 The experimental design involved exposing *S. aureus* to the coated samples of TiO₂-Ag7
206 and TiO₂-Ag7-HA in 24-well, flat-bottom sterile polystyrene plates (Thermo Fischer
207 Scientific, Loughborough, UK). TiO₂-NT coated discs were used as a control for the
208 composite coating effect. Silver nitrate was used as a metal salt control for any possible
209 dissolved silver effect from the coating. Silver nanoparticles alone were also used as a
210 control for Ag NP effect that might arise from the coatings. *S. aureus* was allowed to
211 grow on its own as a negative control. Nine replicate runs were conducted for each type
212 of coated samples and the controls (n = 6 for biochemical assays and n = 3 for SEM).
213 Following the approach by Besinis *et al* (2014a), the materials were exposed to *S. aureus*
214 for 24 h and the proportion of live to dead cells and the amount of lactate produced were
215 evaluated (see biochemical assays below). The concentration of total dissolved silver,
216 calcium and phosphorus released from the coating in the SBF were also measured.

217 *S. aureus* was chosen as it is considered to be one of the main causes of infection
218 in orthopaedic and dental implants (Swank and Dragoo, 2013, Tsikandylakis *et al.*, 2014).

219 *S. aureus* was cultured in brain heart infusion (BHI) broth (Lab M Ltd, Bury, UK) at 37
220 °C. A bacterial suspension having optical density 0.018 at 595 nm absorbance
221 (Spectrophotometer Genesys 20, Fisher Scientific, Loughborough, UK) was prepared in
222 the BHI broth at a concentration of 1×10^7 cells/mL. For the experiments, 2 mL of the
223 bacterial culture was pipetted in each well of a 24-well plate containing TiO₂-NTs, TiO₂-
224 Ag7, TiO₂-Ag7-HA, AgNO₃ (0.001M), or Ag NPs (107.9 mg/L equal to 0.001M)
225 dispersed in ultrapure deionised water on their own (n = 9 replicates of each). A silver
226 concentration of 0.001M was used for the positive controls as it was found that 0.001M
227 was the maximum amount of silver released from the coatings. The 24-well microplates
228 were then incubated at 37 °C on a shaking table. At the end of the overnight exposure, six
229 of the replicate plates were used for biochemistry. An aliquot (1 mL) of the exposed broth
230 from each well were collected for the LIVE/DEAD[®] kit and lactate production assays
231 (see below). The remaining broth was acidified with 70 wt% HNO₃ and used for metal
232 determination. Then the remaining adherent bacterial were collected. Bacterial pellets
233 were obtained whereby the samples from the wells were sonicated (12 MHz) for 60 s in
234 2 mL of sterile saline to remove the bacteria from the discs (Besinis *et al.*, 2014b). Then,
235 1 mL of the resulting suspension were allowed to grow in 5 mL of BHI broth for 5 h at
236 37 °C on a shaking table with the aim of increasing the amount of live cells in order to
237 readily measure them with the Live/Dead assay. The viability of the cells and the amount
238 of lactate in the suspension was also assessed, followed by the measurement of the ionic
239 composition of the latter. For the remaining three replicates, the broth was removed and
240 the samples were prepared for electron microscopy.
241

242 ***Cell viability and lactate production assays***

243 The cell viability of *S. aureus* in both the exposed broth and incubated cell suspension
244 from all of the relevant treatments and controls [TiO₂-NTs, TiO₂-Ag7, TiO₂-Ag7-HA,
245 AgNO₃ (0.001M), and Ag NPs] were assessed using the L7012 LIVE/DEAD®
246 Backlight™ Kit (Invitrogen Ltd, Paisley, UK), exactly according to Gunputh *et al.*
247 (2018). Briefly, 100 µL of the exposed broth and 100 µL of the incubated homogenate
248 from each replicate was subject to several washes with sterile NaCl solution. Then 100
249 µL of the final suspension from each well were used for fluorimetry in clean 96 well
250 plates with 100 µL of freshly prepared dyes from the LIVE/DEAD kit. Microplate were
251 incubated in the dark at room temperature for 15 min and the fluorescence measured on
252 a Cytofluor II fluorescence plate reader (excitation, 485 nm; emission at 530 nm and 645
253 nm). The readings at 530 nm were divided by the readings at 645 nm in order to obtain
254 the percentage of live to dead cells in the exposed broth and the incubated cell suspension
255 from the different samples and controls according to the kit instructions.

256 The metabolic activity of *S. aureus* was assessed by measuring the amount of lactate
257 present in both the exposed broth and incubated cell suspension from the wells containing
258 TiO₂-NTs, TiO₂-Ag7, TiO₂-Ag7-HA, AgNO₃ (0.001M), and Ag NP (6 replicates of each)
259 according to Besinis *et al* (2013). Briefly, 100 µL of the exposed broth, or 100 µL of the
260 incubated homogenate as appropriate, were transferred to a V-bottom 96-well microplate
261 and were centrifuged at 2000 rpm for 10 minutes to generate a clean supernatant that
262 could be measured for total lactate. Then, in a new plate, 1 µL of 1000 units/mL of lactate
263 dehydrogenase (Sigma-Aldrich Ltd, UK) was pipetted into wells of a 96-well plate
264 followed by 10 µL of 40 mmol/L nicotinamide adenine dinucleotide and 200 µL of 0.4
265 mol/L hydrazine prepared in a glycine buffer of pH 9. Ten µL of the supernatants were
266 then added, mixed and incubator at 37°C for 2 hours to allow lactate production to occur.

267 The absorbance was then read at 340 nm against lactic acid as standards (0, 0.25, 0.5, 1.0,
268 2.0, 4.0, 8.0 mmol/L).

269

270 ***Metal analysis following S. aureus exposure***

271 The exposed broth and the detached bacteria were analysed for silver, calcium and
272 phosphorus composition. After the exposure to *S. aureus*, 1 mL of the broth or the
273 detached bacteria were diluted with Milli-Q water to a final volume of 5 mL and acidified
274 (few drops of 70 wt% nitric acid). Total Ag concentrations were determined by
275 inductively coupled plasma mass spectrometry (ICP-MS, Varian 725-ES Melbourne,
276 Australia), and total Ca or P by optical emission spectrometry (ICP-OES, Thermo
277 Scientific XSeries 2, Hemel Hempstead, UK). Calibrations for both instruments were
278 performed with matrix-matched analytical grade standards. For ICP-MS the standards
279 and samples contained internal references (0.5, 0.25 and 1% of iridium) for SBF, broth
280 and any homogenates made from bacteria. In the complex matrix of broth and SBF, the
281 detection limit was around 0.001 µg/L for Ag by ICP-MS, and 5 µg/L for Ca and 40 µg/L
282 for P by ICP-OES.

283

284 ***Imaging of the attached S. aureus***

285 The remaining 3 repeats of the control, TiO₂, TiO₂-Ag7, TiO₂-Ag7-HA, AgNO₃ and Ag
286 NP were examined by scanning electron microscope to confirm the presence of *S. aureus*
287 on the different surfaces. After the 24 h exposure to *S. aureus*, the supernatants were
288 removed and the plates carefully washed twice with sterile saline (0.85 wt% NaCl). Then
289 2 mL of 3 wt% glutaraldehyde in 0.1 mol/L cacodylate buffer was added to each well and
290 was allowed to stay overnight at 4 °C. The next day, the glutaraldehyde was removed and
291 the samples were washed with 0.1 mol/L cacodylate buffer. Specimens were serially

292 dehydrated through ethanol solutions, coated with carbon, and viewed under a
293 JEOL7001F SEM. Each specimen was viewed at three different random locations (i.e., 3
294 images of each specimen x 3 replicate samples). Care was taken to systematically
295 photograph the specimens without bias and at the same magnifications for all treatments.

296

297 ***Statistical analysis***

298 The data from the cell viability assay, the lactate production assay and the ionic
299 concentration measurements were analysed using Statgraphics Centurion XVII (StatPoint
300 Technologies, Inc.). After descriptive statistics, data were checked for normality and for
301 equal variances (Levene's test). When data were parametric, the data was analysed for
302 treatment or time effects using one way ANOVA with Fisher's LSD test post-hoc. In
303 cases of unequal variances, the data were transformed before analysis and where the data
304 remained non-parametric, the Kruskal Wallis test was used. Data are presented as mean
305 \pm S.E.M unless otherwise stated. The default 95% confidence level was used for all
306 statistics.

307 **Results**

308 ***Dialysis experiment and the stability of coatings***

309 Figure 3 shows the results of the dialysis experiments. The total concentration of silver
310 from the samples without any silver coatings was minimal as expected. In the presence
311 of Ag-containing materials, there was a rise in the total Ag concentration in the external
312 compartment of the dialysis bag, reaching a maximum of 5.44 ± 0.06 and 3.27 ± 0.15
313 $\mu\text{g/L}$ from $\text{TiO}_2\text{-Ag7}$ and $\text{TiO}_2\text{-Ag7-HA}$ respectively. The maximum dissolution rates
314 were $0.17 \pm 0.01 \mu\text{g/h}$ and $0.21 \pm 0.05 \mu\text{g/h}$ for Ag from $\text{TiO}_2\text{-Ag7}$ and $\text{TiO}_2\text{-Ag7-HA}$
315 respectively (statistically different, ANOVA, $p < 0.05$, $n = 3$). Figure 3 also shows the

316 dissolution of calcium and phosphorus from the coated samples. A similar trend in the
317 total concentration was observed for both Ca and P in the beaker (Figure 3B and 3C). The
318 maximum concentration of Ca reached was 86.5 ± 1.48 and 92.0 ± 0.36 mg/L from TiO₂-
319 Ag7 and TiO₂-Ag7-HA respectively with a maximum dissolution rate of 68.8 ± 1.92 mg/h
320 and 73.4 ± 0.07 mg/h respectively. The maximum concentration of P reached was $27.6 \pm$
321 0.73 and 28.4 ± 0.24 mg/L from TiO₂-Ag7 and TiO₂-Ag7-HA respectively with a
322 maximum dissolution rate of 21.8 ± 0.42 and 23.0 ± 0.51 mg/h respectively.

323 ***Confirming silver exposure in the broth during S. aureus exposures***

324 The measured total Ag concentrations in the broth during the exposure of *S. aureus* to the
325 different composite coating and relevant controls are shown in Figure 4A. For the controls
326 and materials without silver, as expected they showed only a background concentration
327 of the metal ($6.78 \mu\text{g/L}$). The positive controls of AgNO₃ and Ag NPs alone had a high
328 concentration of silver, 67.7 ± 2.1 and 1.36 ± 0.025 mg/L respectively. Where the coatings
329 contained Ag NPs, total Ag (form unknown) was readily measured in the broth (Figure
330 4A). The broth exposed to both TiO₂-Ag7 and TiO₂-Ag7-HA discs had 2.08 ± 0.2 and
331 0.50 ± 0.1 mg/L of total Ag respectively (significantly less total Ag from TiO₂-Ag7-HA
332 (Kruskal-Wallis, $p < 0.05$; $n = 6$). Thus the coating with HA impeded the release of the
333 majority of the silver from the coatings in the presence of the broth.

334

335 ***Cell morphology and survival***

336 Specimens from the controls and treatments were examined for abundance and
337 morphology of the bacteria by electron microscopy at the end of the experiment (Figure
338 5). As expected the bacteria cultured directly on the plastic wells (control) survived and
339 grew on the whole surface (Figure 5A). The bacteria also grew on the TiO₂-NTs (Figure
340 5B), but were sparse or absent on all the Ag-containing materials (Figures 5C-F). The

341 electron microscopy observations were consistent with by the proportions of live bacteria
342 detected using the L7012 LIVE/DEAD[®] Backlight[™] Kit after a 24 h of exposure to the
343 composite materials or the controls (Figure 6). The percentage of live bacteria was high
344 in the broth ($72.5 \pm 2.9\%$) and on the surface of the plastic well ($100.9 \pm 2.6\%$), as
345 expected. The control cells were the most metabolically active compared to all other
346 treatments (Kruskal Wallis, $p < 0.05$, $n = 6$) as confirmed by the lactate production assay
347 (Figures 6C-D).

348 Slightly few bacteria grew on the TiO₂-NTs, but with >80% alive on the surface
349 this material was not biocidal. In contrast, the bacteria exposed to silver controls (AgNO₃
350 or dispersions of Ag NP) were dead (< 1% live bacteria) and with negligible lactate
351 production (0.2 mM or much less, Figure 6). AgNO₃ and Ag NPs were equally effective
352 biocides (not statistically different from each other, Figure 6). Both TiO₂-Ag7 and TiO₂-
353 Ag7–HA coatings had a significantly lower percentage of live to dead cells ($6.74 \pm 0.98\%$
354 and $1.78 \pm 0.29\%$ respectively) as compared to the control or TiO₂-NTs. The TiO₂-Ag7
355 was as effective as AgNO₃ or dispersions of Ag NPs at killing bacteria with only $3.4 \pm$
356 0.3% live on the former and negligible lactate production (Figures 6A and C). Notably,
357 with the addition of nHA, the TiO₂-Ag7–HA coating still retained most of its biocidal
358 properties with $13.9 \pm 1.0\%$ of live cells attached to its surface and only 1.07 ± 0.03 mM
359 of lactate production (Figures 6A and C).

360 **Discussion**

361 *Improved fabrication and Ag release from the composite coating*

362 In this study, TiO₂-NTs were successfully decorated with a uniform distribution of
363 individual Ag NPs on the surface (Figure 1C). This is a marked improvement on our
364 previous attempts to reduce silver ions to Ag NPs on the surface of TiO₂-NTs using the

365 biocompatible reducing agent, δ -gluconolactone (Gunpath *et al.*, 2018), where the
 366 distribution of the nanoparticles was not uniform and showed micron and nano-sized
 367 clusters of the particles. Furthermore, in the present study the as formed TiO₂-NTs were
 368 initially treated at 350 °C to increase their chemical stability (Zazpe *et al.*, 2017) followed
 369 by an alkaline treatment in 2 mol/L NaOH which made the nanotube more receptive to
 370 silver ammonia solution. When the TiO₂-NTs react with NaOH, sodium titanate crystals
 371 are formed on the nanotubes (Tsai and Teng, 2006) as per Equation (1):

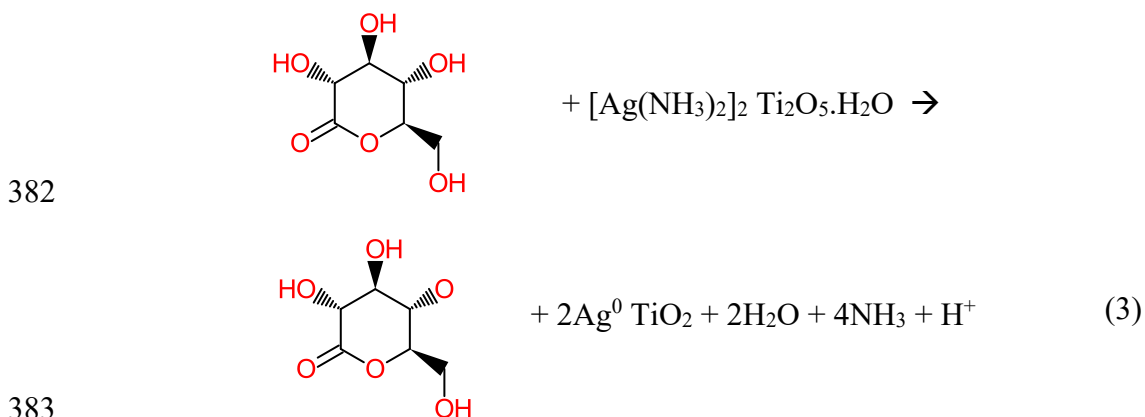


373 When exposed to silver ammonia solution, the Na⁺ is substituted by the silver ammonia
 374 complex as per Equation (2) (Gunpath *et al.*, 2018).



376 The latter attachment of the silver ammonia to titanate is stronger than the bond in the
 377 TiO₂-[Ag(NH₃)₂]⁺ complex (Gunpath *et al.*, 2018). Hence, the exposure to δ -
 378 gluconolactone reduced the silver complexes to silver nanoparticles still attached to the
 379 nanotubes as per Equations (3) below.

380
 381



384 In the presence of δ -gluconolactone, the silver ammonia, while still being attached to the
 385 nanotubes, is reduced to Ag NPs. Hence, the decoration is achieved, and by modifying

386 the incubation time the clustering and size of the Ag NPs can be controlled (Gunpath *et*
387 *al.*, 2018). In the present study this was optimised, with the TiO₂-Ag7, achieving the
388 desired decoration (Figure 1C). Further details on the stability of the TiO₂-NTs such as
389 the current density, porosity, pH effects, and Gibbs free energy can be found elsewhere
390 (Danookdharree *et al.*, 2015). The absence of high Ag concentrations in the broth at the
391 end of the experiment also suggests the TiO₂-NTs with their Ag NP decoration was
392 remaining attached to the Ti alloy. The visible presence of Ag NPs on the materials
393 (Figure 1) argues that the Ag is remaining in the reduced form, Ag⁰, as expected from x-
394 ray photoelectron spectroscopy (XPS) studies of Ag NPs grown on TiO₂ materials
395 (Kamaraj *et al.*, 2015). Also, the low µg/L releases of Ag by dissolution, suggests very
396 little of the Ag is oxidising (i.e., as assumed soluble Ag⁺), and in any event it will
397 spontaneously form sparingly soluble AgCl complexes in the media (Besinis *et al.*,
398 2014a), not silver oxides.

399 For biocidal properties, it is desirable to have a slow release of Ag from the surface
400 of the material. This was achieved with the Ag NPs alone decorated on TiO₂-NTs,
401 releasing µg/L amounts of total Ag into the surrounding biological media (Figures 3 and
402 4). However, the osteoblasts critical to the healing of bone show toxicity and lose around
403 75% of their vital alkaline phosphatase activity when in direct contact with Ag NPs on
404 TiO₂-NTs (Zhao *et al.*, 2011). So, our approach was to include a top coat of nHA, which
405 still allowed some release of dissolved Ag in dialysis experiments with SBF (Figure 3)
406 and into the broth during exposure to *S. aureus* (Figure 4).

407

408 ***Antibacterial properties***

409 In the present study, as expected, the TiO₂-Ag7 coating was biocidal with almost no live
410 bacteria attached to the surface or remaining suspended in the broth (Figures 5 and 6).

411 Indeed, the TiO₂-Ag7 coating was as potent as AgNO₃ solution or dispersions of free Ag
412 NPs (Figures 5 and 6). The biocidal properties in this circumstance could arise either from
413 direct contact toxicity of the Ag NPs on the cell walls of the bacteria, or from any
414 dissolved Ag released (Reidy *et al.*, 2013). It is also theoretically possible for UV light
415 stimulation to catalyse the oxidation of some Ag⁰ with TiO₂ to form reactive oxygen
416 species that subsequently kill bacteria (Hajjaji *et al.*, 2018), although this is not relevant
417 to the conditions here. Regardless of mechanisms, there are few reports of the MIC values
418 for Ag NPs suspensions with *S. aureus*. Yuan *et al.* (2017) reported an MIC of 2 µg/mL
419 for a multi-drug resistant strain of *S. aureus*. Similarly for methicillin-resistant *S. aureus*
420 (MRSA), Paredes *et al.* (2014) reported MIC values of around 0.25 µg/mL for Ag NPs.
421 Although neither of these latter studies included silver salt controls or particle dissolution
422 measurements, it suggests that low mg/L concentrations of Ag NPs are biocidal, as
423 observed here (Figures 5 and 6). Dissolved silver is arguably more toxic and as little as
424 50 µg/L can completely kill *S. aureus* in 24 h in physiological saline (Jung *et al.*, 2008).
425 In the present study, dissolution of 2-3 µg/L of dissolved Ag was demonstrated in the
426 dialysis experiments with TiO₂-Ag7 (Figure 3), and this material showed no appreciable
427 microbial biofilm (Figure 5). This magnitude of apparent dissolved Ag release is also far
428 below the acute toxicity values for mammalian cells. For example, fibroblasts have an
429 EC50 of 1.7 mg/L for AgNO₃ and between 17-35 mg/L for Ag NPs depending on particle
430 size (Ivask *et al.*, 2014). Bone cement loaded with up to 1% w/v as Ag NPs also has no
431 appreciable toxicity to osteoblasts *in vitro* (Alt *et al.*, 2004). Thus the silver release is
432 biocidal, but not likely to be toxic to the surrounding human tissue.

433 The presence of a nHA top coat did not hinder the antibacterial properties of the
434 implant material (Figure 5). The nHA formed a consistent layer over the TiO₂-NTs
435 decorated with Ag NPs, but with some cracks in the nHA surface (Figure 2). This has

436 been observed before with nHA coatings and is likely due to differences in the thermal
437 expansion coefficients of nHA compared to the underlying materials (Besinis *et al.*,
438 2017). The small fissures in the nHA coat serve to enable the controlled release of the
439 underlying silver (e.g., from electroplated titanium alloy, (Besinis *et al.*, 2017) and a
440 similar observation was made here with the TiO₂-Ag7-HA treatment (Figures 3 and 4).
441 Thus overall, the fissures in the nHA top coating are a desirable feature that enable the
442 leaching of some Ag to cause antimicrobial properties towards *S. aureus*, and yet the nHA
443 would also provide a known biocompatible surface for human osteoblasts.

444 In conclusion, the chemical reduction of silver ammonia using δ -gluconolactone
445 was successfully used to synthesise individual Ag NPs that consistently decorated the
446 surface of TiO₂-NTs. Both TiO₂-Ag7 and TiO₂-Ag7-HA exhibited antibacterial
447 properties, but the latter material with a nHA top coat is more desirable from the
448 viewpoint of biocompatibility with human cells. The next step in the research will be to
449 explore the adherence and differentiation of osteoblasts on the TiO₂-Ag7-HA with a view
450 to demonstrating osseointegration of the implant material with human bone.

451

452 **Acknowledgements**

453 Technical support from the Schools of Marine Science and Engineering, Biological and
454 Biomedical Sciences, and the Electron Microscopy Centre (EMC) at Plymouth University
455 is gratefully acknowledged.

456

457 **Disclosure Statement**

458 There are no conflicts of interest.

459

460 **Funding**

461 UG was supported by a joint PhD studentship from the Faculty of Science and
462 Environment and the Peninsular Schools of Medicine and Dentistry.

463

464 **References**

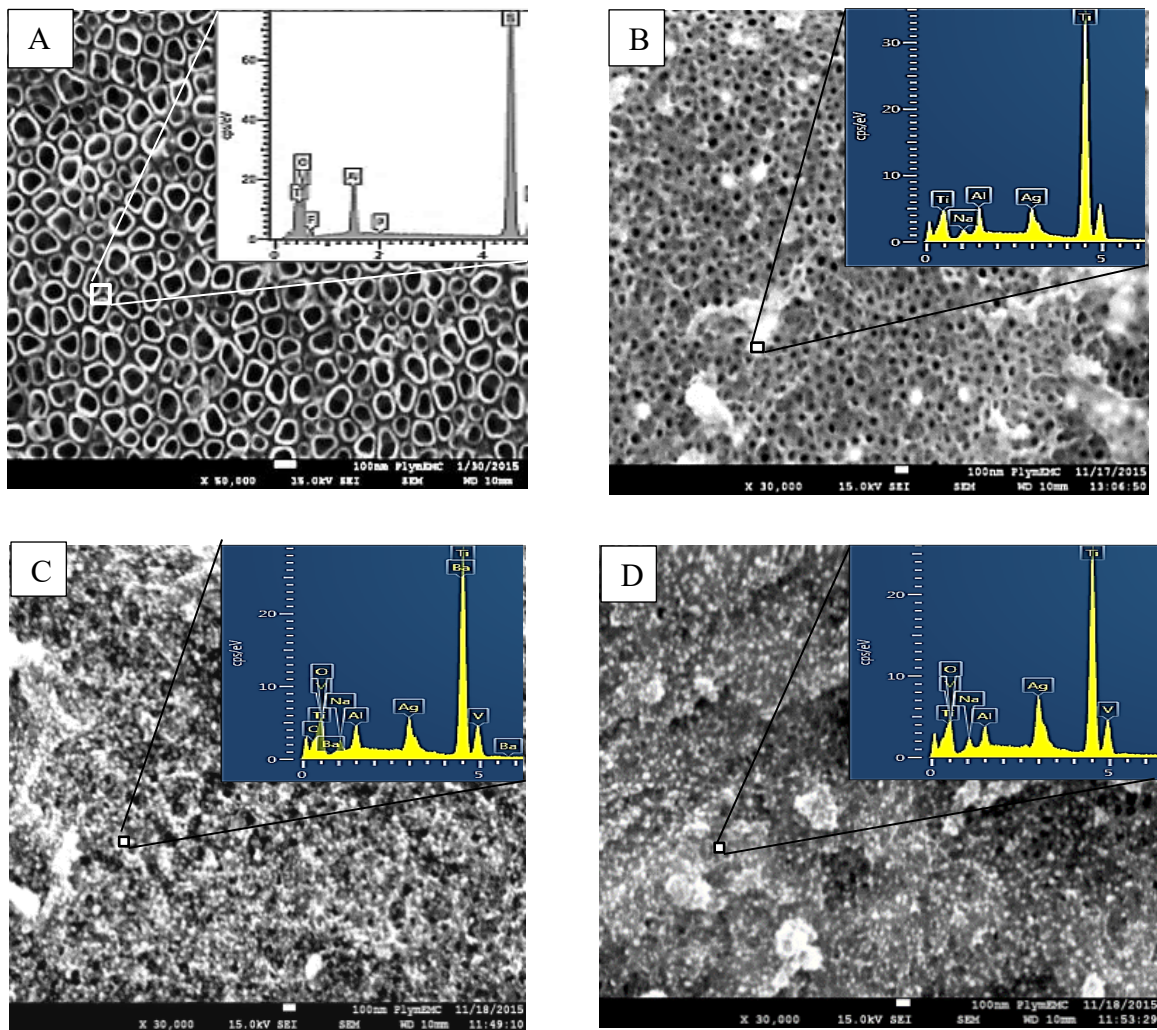
- 465 Alt, V., Bechert, T., Steinrücke, P., Wagener, M., Seidel, P., Dingeldein, E., Domann,
466 E. & Schnettler, R., 2004. An *in vitro* assessment of the antibacterial properties
467 and cytotoxicity of nanoparticulate silver bone cement. *Biomaterials*, 25, 4383-
468 4391.
- 469 Balani, K., Anderson, R., Laha, T., Andara, M., Tercero, J., Crumpler, E. & Agarwal,
470 A., 2007. Plasma-sprayed carbon nanotube reinforced hydroxyapatite coatings
471 and their interaction with human osteoblasts *in vitro*. *Biomaterials*, 28, 618-624.
- 472 Besinis, A., De Peralta, T. & Handy, R.D., 2014a. The antibacterial effects of silver,
473 titanium dioxide and silica dioxide nanoparticles compared to the dental
474 disinfectant chlorhexidine on *Streptococcus mutans* using a suite of bioassays.
475 *Nanotoxicology*, 8, 1-16.
- 476 Besinis, A., De Peralta, T. & Handy, R.D., 2014b. Inhibition of biofilm formation and
477 antibacterial properties of a silver nano-coating on human dentine.
478 *Nanotoxicology*, 8, 745-754.
- 479 Besinis, A., Hadi, S.D., Le, H.R., Tredwin, C. & Handy, R.D., 2017. Antibacterial
480 activity and biofilm inhibition by surface modified titanium alloy medical
481 implants following application of silver, titanium dioxide and hydroxyapatite
482 nanocoatings. *Nanotoxicology*, 11, 327-338.
- 483 Brammer, K.S., Frandsen, C.J. & Jin, S., 2012. TiO₂ nanotubes for bone regeneration.
484 *Trends in Biotechnology*, 30, 315-22.
- 485 Chernozem, R.V., Surmeneva, M.A., Krause, B., Baumbach, T., Ignatov, V.P., Prymak,
486 O., Loza, K., Epple, M., Ennen-Roth, F. & Wittmar, A., 2019. Functionalization
487 of titania nanotubes with electrophoretically deposited silver and calcium
488 phosphate nanoparticles: structure, composition and antibacterial assay.
489 *Materials Science and Engineering: C*, 97, 420-430.
- 490 Chernozem, R.V., Surmeneva, M.A., Krause, B., Baumbach, T., Ignatov, V.P., Tyurin,
491 A.I., Loza, K., Epple, M. & Surmenev, R.A., 2017. Hybrid biocomposites based
492 on titania nanotubes and a hydroxyapatite coating deposited by RF-magnetron
493 sputtering: Surface topography, structure, and mechanical properties. *Applied*
494 *Surface Science*, 426, 229-237.
- 495 Connaughton, A., Childs, A., Dylewski, S. & Sabesan, V.J., 2014. Biofilm disrupting
496 technology for orthopedic implants: what's on the horizon? *Frontiers in*
497 *Medicine (Lausanne)*, 1, 22.
- 498 Danookdharree, U., Le, H. & Tredwin, C., 2015. The effect of initial etching sites on
499 the morphology of TiO₂ nanotubes on Ti-6Al-4V alloy. *Journal of the*
500 *Electrochemical Society*, 162, E213-E222.
- 501 Descamps, S., Awitor, K.O., Raspal, V., Johnson, M.B., Bokalawela, R.S.P., Larson,
502 P.R. & Doiron, C.F., 2013. Mechanical properties of nanotextured titanium
503 orthopedic screws for clinical applications. *Journal of Medical Devices*, 7,
504 0210051-0210055.
- 505 Gao, A., Hang, R., Huang, X., Zhao, L., Zhang, X., Wang, L., Tang, B., Ma, S. & Chu,
506 P.K., 2014. The effects of titania nanotubes with embedded silver oxide
507 nanoparticles on bacteria and osteoblasts. *Biomaterials*, 35, 4223-35.
- 508 Gunputh, U.F., Le, H., Handy, R.D. & Tredwin, C., 2018. Anodised TiO₂ nanotubes as
509 a scaffold for antibacterial silver nanoparticles on titanium implants. *Materials*
510 *Science and Engineering: C*, 91, 638-644.

- 511 Ha, S.-W., Jang, H.L., Nam, K.T. & Beck, G.R., 2015. Nano-hydroxyapatite modulates
512 osteoblast lineage commitment by stimulation of DNA methylation and
513 regulation of gene expression. *Biomaterials*, 65, 32-42.
- 514 Hajjaji, A., Elabidi, M., Trabelsi, K., Assadi, A., Bessais, B. & Rtimi, S., 2018.
515 Bacterial adhesion and inactivation on Ag decorated TiO₂-nanotubes under
516 visible light: Effect of the nanotubes geometry on the photocatalytic activity.
517 *Colloids and Surfaces B: Biointerfaces*, 170, 92-98.
- 518 Ivask, A., Kurvet, I., Kasemets, K., Blinova, I., Aruoja, V., Suppi, S., Vija, H., Käkinen,
519 A., Titma, T. & Heinlaan, M., 2014. Size-dependent toxicity of silver
520 nanoparticles to bacteria, yeast, algae, crustaceans and mammalian cells *in vitro*.
521 *PloS one*, 9, e102108.
- 522 Jung, W.K., Koo, H.C., Kim, K.W., Shin, S., Kim, S.H. & Park, Y.H., 2008.
523 Antibacterial activity and mechanism of action of the silver ion in
524 *Staphylococcus aureus* and *Escherichia coli*. *Applied and Environmental*
525 *Microbiology*, 74, 2171-2178.
- 526 Kamaraj, K., George, R., Anandkumar, B., Parvathavarthini, N. & Mudali, U.K., 2015.
527 A silver nanoparticle loaded TiO₂ nanoporous layer for visible light induced
528 antimicrobial applications. *Bioelectrochemistry*, 106, 290-297.
- 529 Kokubo, T., Kushitani, H., Sakka, S., Kitsugi, T. & Yamamuro, T., 1990. Solutions able
530 to reproduce *in vivo* surface-structure changes in bioactive glass-ceramic A-W3.
531 *Journal of Biomedical Materials Research*, 24, 721-734.
- 532 Meyerink, J.G., Kota, D., Wood, S.T. & Crawford, G.A., 2018. Transparent titanium
533 dioxide nanotubes: Processing, characterization, and application in establishing
534 cellular response mechanisms. *Acta biomaterialia*, 79, 364-374.
- 535 Moriarty, T.F., Kuehl, R., Coenye, T., Metsemakers, W.-J., Morgenstern, M., Schwarz,
536 E.M., Riool, M., Zaat, S.a.J., Khana, N., Kates, S.L. & Richards, R.G., 2016.
537 Orthopaedic device-related infection: current and future interventions for
538 improved prevention and treatment. *EFORT Open Reviews*, 1, 89-99.
- 539 Nie, B., Long, T., Ao, H., Zhou, J., Tang, T. & Yue, B., 2017. Covalent immobilization
540 of enoxacin onto titanium implant surfaces for inhibiting multiple bacterial
541 species infection and *in vivo* methicillin-resistant *Staphylococcus aureus*
542 infection prophylaxis. *Antimicrobial Agents and Chemotherapy*, 61, e01766-16.
- 543 O'brien, F.J., 2011. Biomaterials & scaffolds for tissue engineering. *Materials Today*,
544 14, 88-95.
- 545 Parcharoen, Y., Kajitvichyanukul, P., Sirivisoot, S. & Termsuksawad, P., 2014.
546 Hydroxyapatite electrodeposition on anodized titanium nanotubes for orthopedic
547 applications. *Applied Surface Science*, 311, 54-61.
- 548 Paredes, D., Ortiz, C. & Torres, R., 2014. Synthesis, characterization, and evaluation of
549 antibacterial effect of Ag nanoparticles against *Escherichia coli* O157:H7 and
550 methicillin-resistant *Staphylococcus aureus* (MRSA). *International Journal of*
551 *Nanomedicine*, 9, 1717-1729.
- 552 Ramires, P.A., Romito, A., Cosentino, F. & Milella, E., 2001. The influence of
553 titania/hydroxyapatite composite coatings on *in vitro* osteoblasts behaviour.
554 *Biomaterials*, 22, 1467-1474.
- 555 Reidy, B., Haase, A., Luch, A., Dawson, K. & Lynch, I., 2013. Mechanisms of silver
556 nanoparticle release, transformation and toxicity: a critical review of current
557 knowledge and recommendations for future studies and applications. *Materials*,
558 6, 2295.

- 559 Rodríguez-Cano, A., Pacha-Olivenza, M.-Á., Babiano, R., Cintas, P. & González-
560 Martín, M.-L., 2014. Non-covalent derivatization of aminosilanized titanium
561 alloy implants. *Surface and Coatings Technology*, 245, 66-73.
- 562 Spriano, S., Yamaguchi, S., Bairo, F. & Ferraris, S., 2018. A critical review of
563 multifunctional titanium surfaces: New frontiers for improving osseointegration
564 and host response, avoiding bacteria contamination. *Acta Biomaterialia*, 79, 1-
565 22.
- 566 Swank, K. & Drago, J.L., 2013. Postarthroscopic infection in the knee following
567 medical or dental procedures. *Case Reports in Orthopedics*, 2013, 974017.
- 568 Tsai, C.-C. & Teng, H., 2006. Structural features of nanotubes synthesized from NaOH
569 treatment on TiO₂ with different post-treatments. *Chemistry of Materials*, 18,
570 367-373.
- 571 Tsikandylakis, G., Berlin, O. & Branemark, R., 2014. Implant survival, adverse events,
572 and bone remodeling of osseointegrated percutaneous implants for transhumeral
573 amputees. *Clinical Orthopaedics and Related Research*, 472, 2947-56.
- 574 Yang, Y., Ao, H.-Y., Yang, S.-B., Wang, Y.-G., Lin, W.-T., Yu, Z.-F. & Tang, T.-T.,
575 2016. *In vivo* evaluation of the anti-infection potential of gentamicin-loaded
576 nanotubes on titania implants. *International Journal of Nanomedicine*, 11, 2223-
577 2234.
- 578 Yuan, Y.-G., Peng, Q.-L. & Gurunathan, S., 2017. Effects of silver nanoparticles on
579 multiple drug-resistant strains of *Staphylococcus aureus* and *Pseudomonas*
580 *aeruginosa* from mastitis-infected goats: An alternative approach for
581 antimicrobial therapy. *International Journal of Molecular Sciences*, 18, 569.
- 582 Zazpe, R., Prikryl, J., Gärtnerova, V., Nechvilova, K., Benes, L., Strizik, L., Jäger, A.,
583 Bosund, M., Sopha, H. & Macak, J.M., 2017. Atomic layer deposition Al₂O₃
584 coatings significantly improve thermal, chemical, and mechanical stability of
585 anodic TiO₂ nanotube layers. *Langmuir*, 33, 3208-3216.
- 586 Zhang, H., Sun, Y., Tian, A., Xue, X.X., Wang, L., Alquhali, A. & Bai, X., 2013.
587 Improved antibacterial activity and biocompatibility on vancomycin-loaded
588 TiO₂ nanotubes: *in vivo* and *in vitro* studies. *International Journal of*
589 *Nanomedicine*, 8, 4379-4389.
- 590 Zhao, L., Wang, H., Huo, K., Cui, L., Zhang, W., Ni, H., Zhang, Y., Wu, Z. & Chu,
591 P.K., 2011. Antibacterial nano-structured titania coating incorporated with silver
592 nanoparticles. *Biomaterials*, 32, 5706-16.

593

594



595 Figure 1: SEM images of Ti-6Al-4V discs coated with (A) TiO₂ nanotubes (×50 000),
 596 (B) TiO₂-Ag₃ (×30 000), (C) TiO₂-Ag₇ (×30 000), (D) TiO₂-Ag₁₀ (×30 000) for
 597 incubations of 3, 7 and 10 minutes in silver ammonia solution respectively. The respective
 598 EDS analysis are of the Ag NPs formed on the surface represented by white spheres/dots
 599 in the images (example images from n = 3 preparations).

TiO₂-Ag7

TiO₂-Ag7-HA

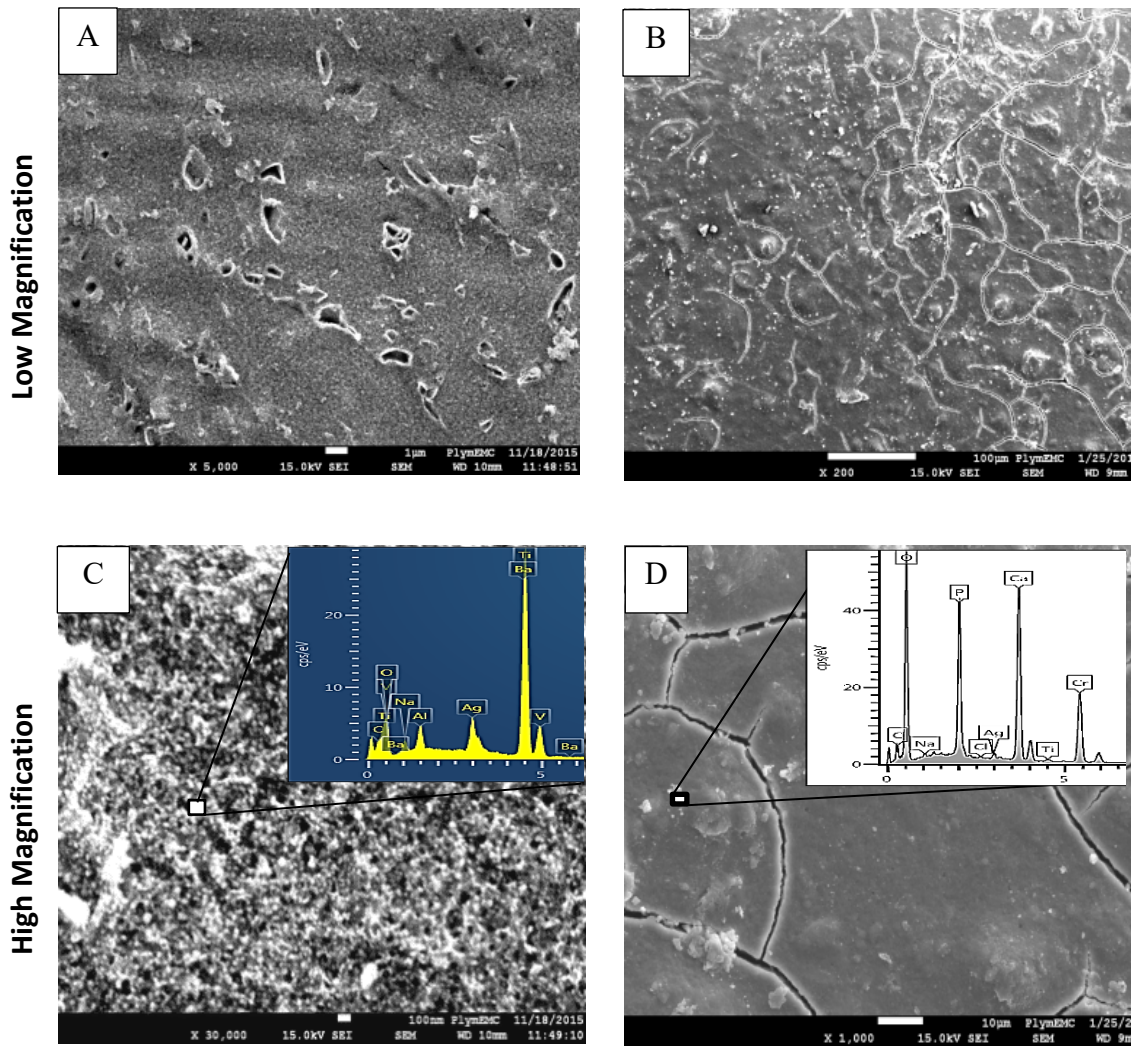


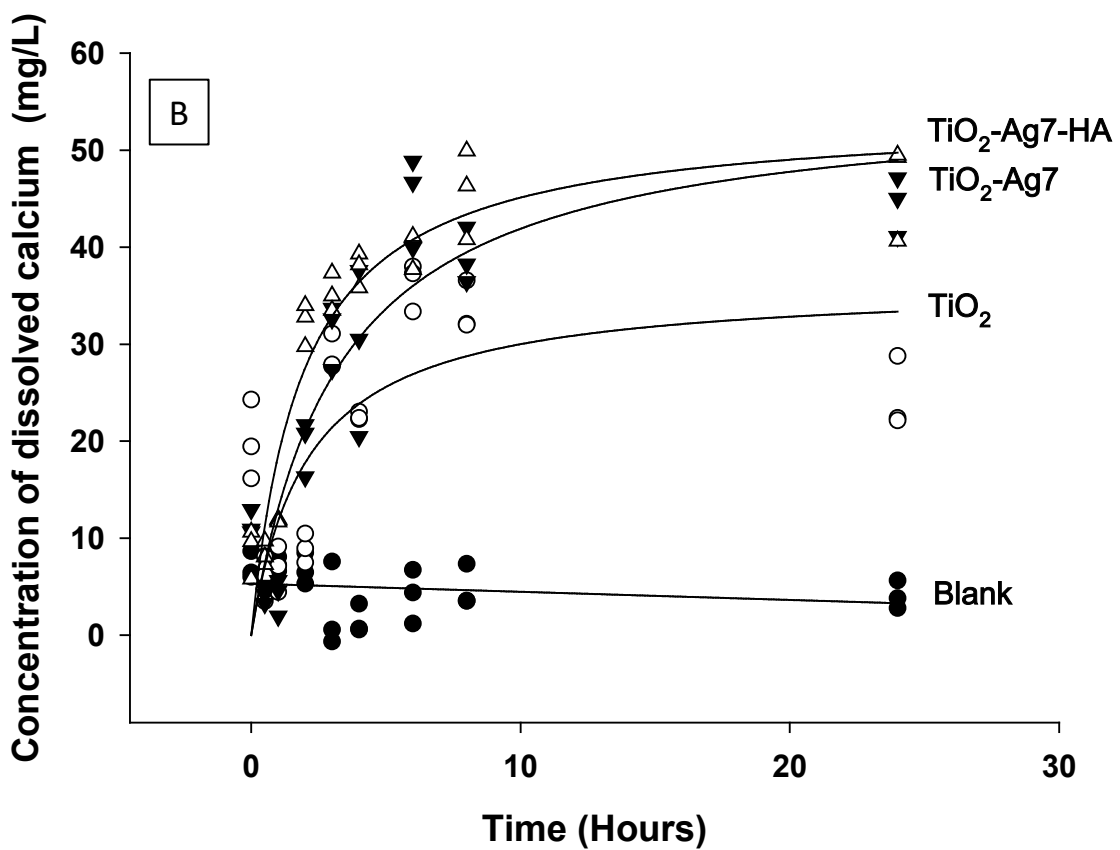
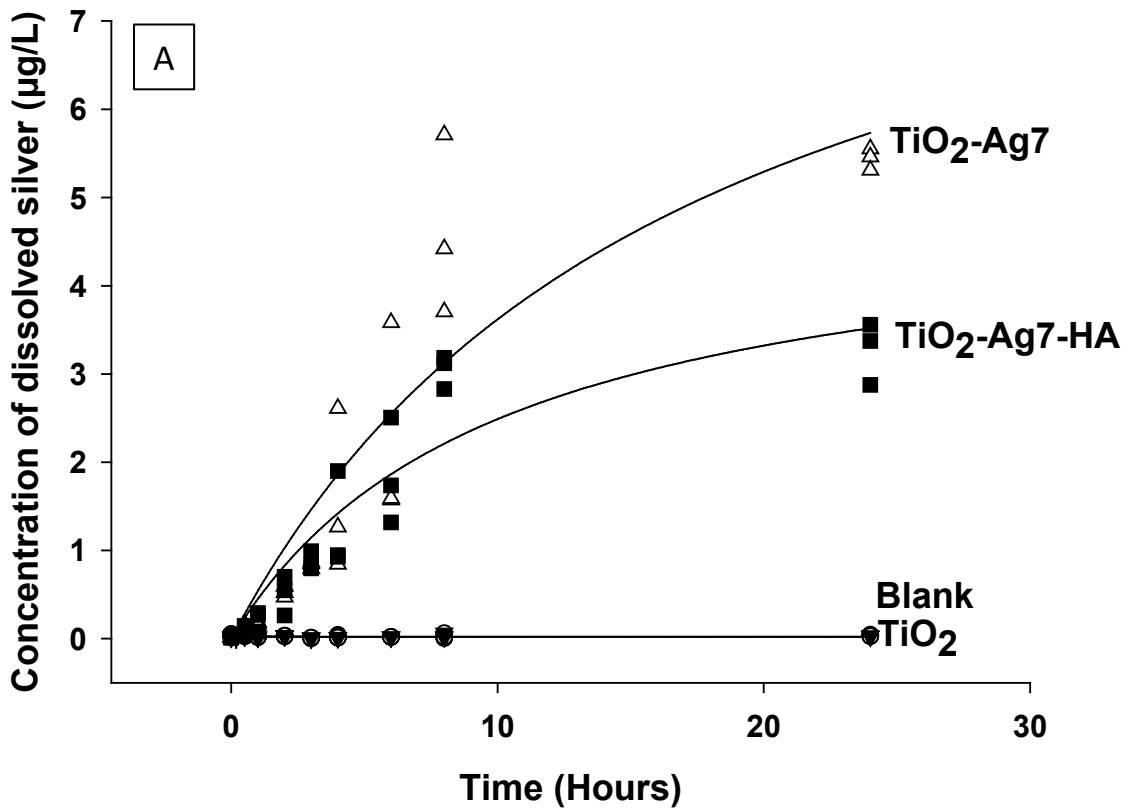
Figure 2: SEM images of (A) TiO₂-Ag7 (×5000) and (B) TiO₂-Ag7-HA (×200) at low magnifications to show coverage of the surface, and their magnified versions in (C, ×30 000) and (D, ×1000) respectively with EDS spectra confirming the expected elemental composition (example images from n = 3 preparations).

600

601

602

603
604
605
606
607
608
609
610
611
612
613
614
615
616
617
618
619
620
621
622
623
624
625
626
627
628
629
630
631
632
633
634
635
636
637
638
639
640
641
642
643
644
645
646



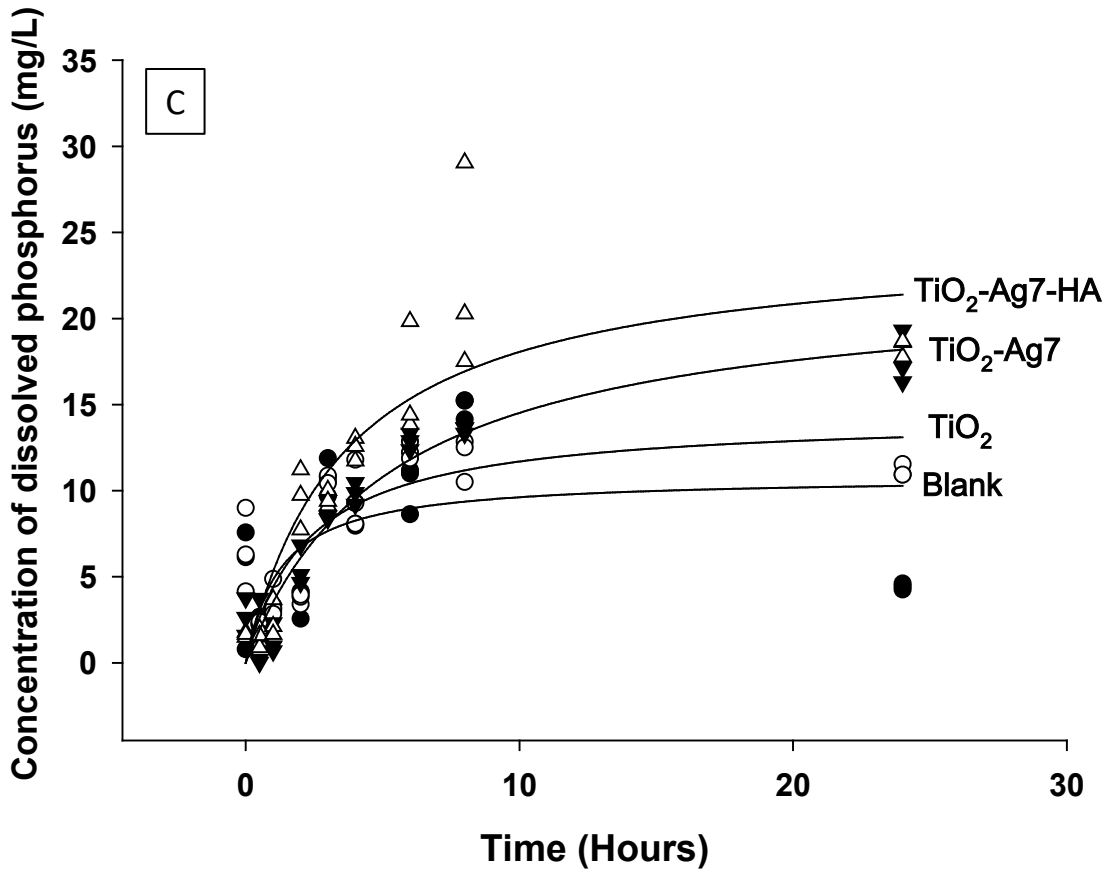


Figure 3: Concentration of (A) total dissolved silver, (B) calcium, and (C) phosphorus measured in simulated body fluid following dialysis of a well without any disc, titanium alloy discs coated with TiO₂ (TiO₂-NTs), TiO₂-Ag7 (TiO₂-NTs decorated with Ag NPs), and TiO₂-Ag7-HA (TiO₂-NTs decorated with Ag NPs, and then a coating of nano hydroxyapatite). Dialysis experiments were performed in triplicate and a rectangular hyperbola function was fitted to the raw data points using Sigmaplot.

677

678

679

680

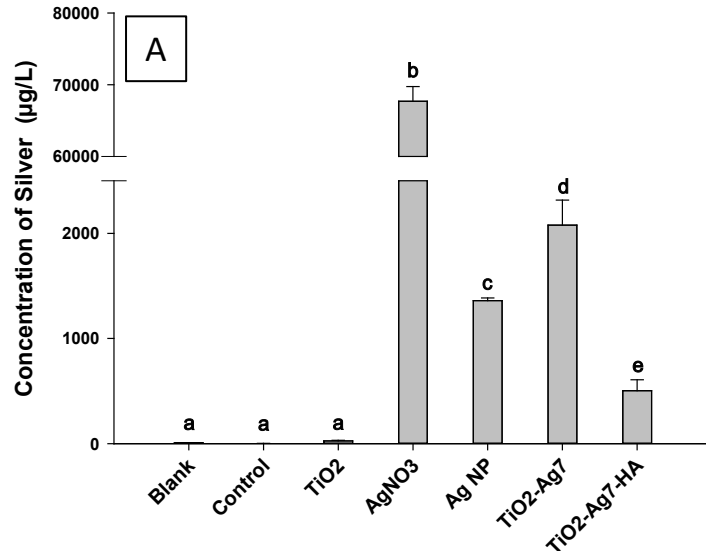
681

682

683

684

685



686

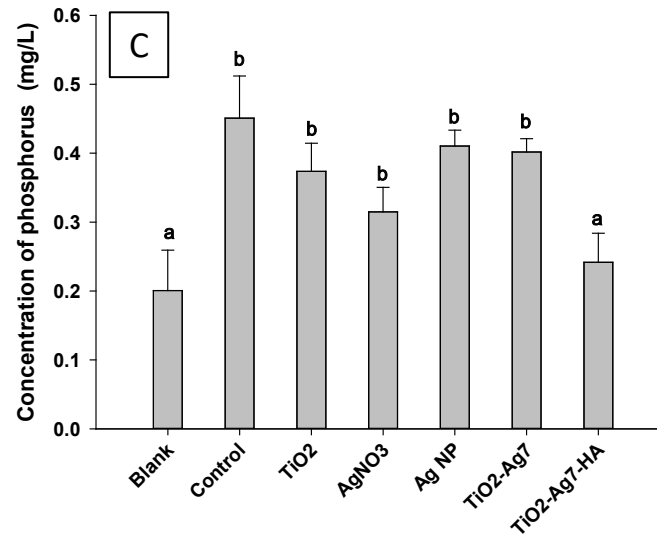
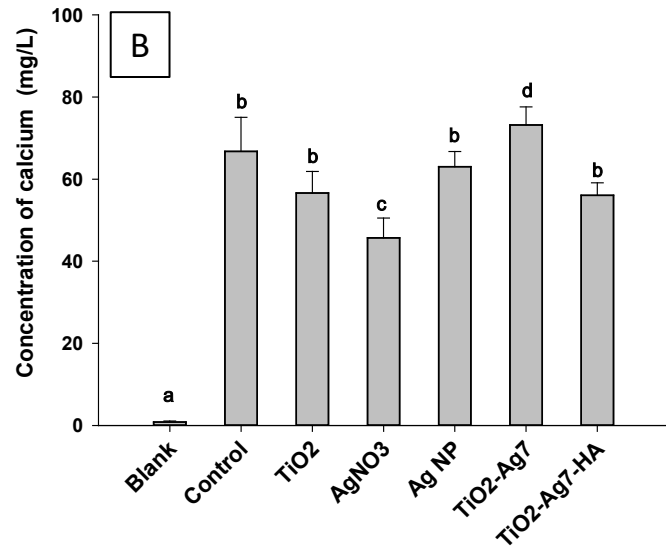
687

688

689

690

691



692 Figure 4: Concentration of (A) total silver, (B) calcium, and (C) phosphorus in the exposed broth after overnight growth of *S. aureus* on: Blank
693 (control with no Ti alloy disc, cells grown directly on the plastic culture plate), TiO₂ (TiO₂-NTs), TiO₂-Ag7 (TiO₂-NTs decorated with Ag NPs),
694 and TiO₂-Ag7-HA (TiO₂-NTs decorated with Ag NPs, and then a coating of nano hydroxyapatite). AgNO₃ and Ag NPs are silver controls, where
695 the bacteria were grown in broth with silver nitrate solution or a dispersion of Ag NPs (i.e., not as a coating). Values are means ± SEM, n = 6
696 replicates. Different letters indicate a statistically significant difference between treatments ($P < 0.05$, Kruskal-Wallis).

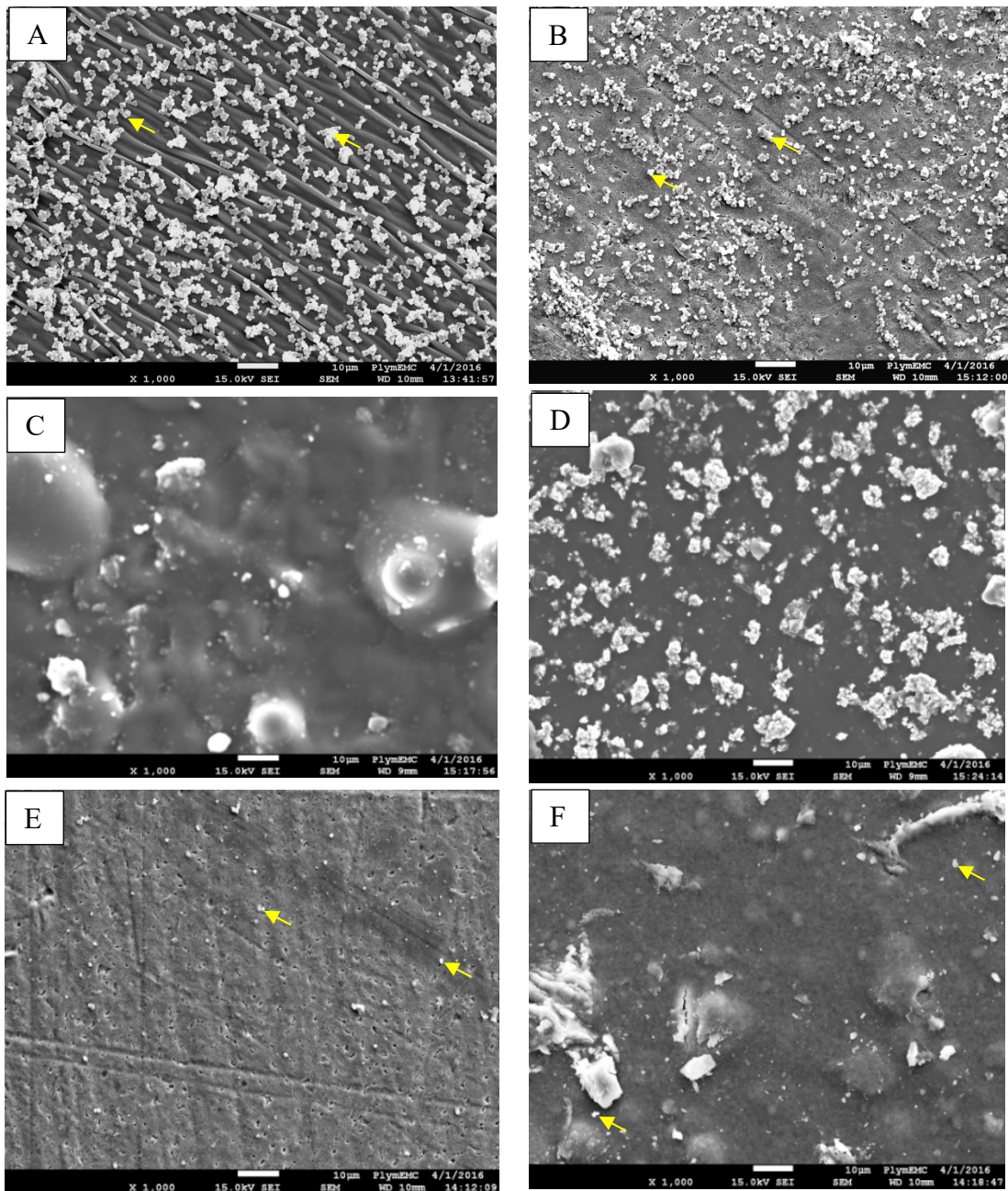
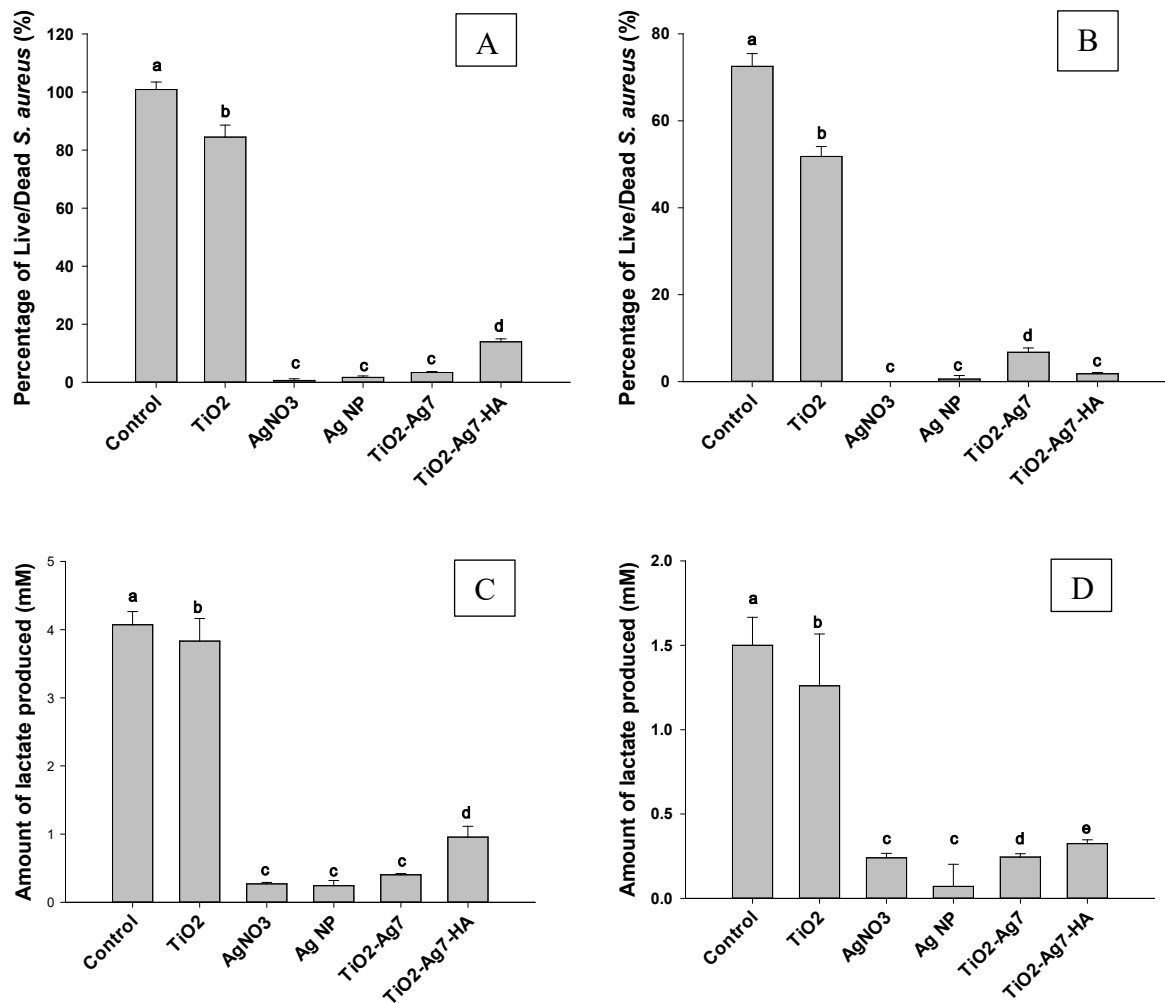


Figure 5: SEM images of attached *S. aureus* (white spherical structures as shown by arrows) after overnight culture in 24-well microplates: (A) Blank (control with no Ti alloy disc, cells grown directly on the plastic culture plate), (B) Ti alloy with TiO₂ nanotubes on the surface (TiO₂-NTs), (C) AgNO₃ solution, (D) Ag NPs in suspension, (E) TiO₂-NTs decorated with Ag NPs (TiO₂-Ag7), and (F) TiO₂-NTs decorated with Ag NPs, and then a coating of nano hydroxyapatite (TiO₂-Ag7-HA). Note, the AgNO₃ and Ag NPs in suspension are silver controls, where the bacteria were grown with the substances added to the broth (i.e., not as a coating).



700

701 Figure 6: The proportion of live to dead *S. aureus* (panels A and B) and lactate production
 702 (panels C and D) by the organism after 24 h when attached to the surface of the materials
 703 (left hand panels), or remaining suspended in the broth (right hand panels). Blank (control
 704 with no Ti alloy disc, cells grown directly on the plastic culture plate), TiO₂ (TiO₂-NTs),
 705 TiO₂-Ag7 (TiO₂-NTs decorated with Ag NPs), and TiO₂-Ag7-HA (TiO₂-NTs decorated
 706 with Ag NPs, and then a coating of nano hydroxyapatite). AgNO₃ and Ag NPs are silver
 707 controls, where the bacteria were grown in broth with silver nitrate solution or a
 708 dispersion of Ag NPs (i.e., not as a coating). Values are means ± SEM, n = 6 replicates.
 709 Different letters indicate a statistically significant difference between treatments (P <
 710 0.05, Kruskal-Wallis).